Radiology

Bachir Taouli, MD
Valérie Vilgrain, MD
Erik Dumont, PhD
Jean-Luc Daire, PhD
Bo Fan, MD
Yves Menu, MD

Index terms:
Liver, diseases, 761.30, 761.79
Liver, focal nodular hyperplasia, 761.3198
Liver neoplasms, 761.30
Liver neoplasms, MR, 761.121416, 761.12144
Magnetic resonance (MR), diffusion study, 761.12144
Magnetic resonance (MR), echo planar, 761.121416

Published online before print
10.1148/radiol.2261011904
Radiology 2003; 226:71–78

Abbreviations:
ADC = apparent diffusion coefficient
HCC = hepatocellular carcinoma

[1] From the Department of Radiology, Hôpital Beaujon and Laboratoire d'Imagerie Médicale Paris-Nord, Faculté de Médecine Paris VII, Clichy, France (B.T., V.V., E.D., J.L.D., Y.M.); and Department of Radiology, University of California San Francisco, 505 Parnassus Ave, Rm M-372, Box 0628, San Francisco, CA 94143 (B.T., B.F.). From the 2001 RSNA scientific assembly. Received November 27, 2001; revision requested February 7, 2002; revision received March 15; accepted May 7. Supported by a grant from the French Radiology Society. **Address correspondence to** B.T. (e-mail: *bachir.taouli@radiology.ucsf.edu*).

Author contributions:
Guarantors of integrity of entire study, V.V., B.T., E.D., Y.M.; study concepts and design, B.T., V.V., E.D., J.L.D.; literature research, B.T., J.L.D.; clinical studies, B.T.; experimental studies, B.T., E.D.; data acquisition, B.T.; data analysis/interpretation, B.T., V.V., B.F.; statistical analysis, B.T., E.D., B.F.; manuscript preparation, B.T.; manuscript definition of intellectual content, V.V., E.D., B.T., Y.M.; manuscript editing, B.T.; manuscript revision/review, B.T., V.V., E.D.; manuscript final version approval, B.T.

Evaluation of Liver Diffusion Isotropy and Characterization of Focal Hepatic Lesions with Two Single-Shot Echo-planar MR Imaging Sequences: Prospective Study in 66 Patients[1]

PURPOSE: To *(a)* evaluate liver diffusion isotropy, *(b)* compare two diffusion-weighted magnetic resonance (MR) imaging sequences for the characterization of focal hepatic lesions by using two or four *b* values, and *(c)* determine an apparent diffusion coefficient (ADC) threshold value to differentiate benign from malignant lesions.

MATERIALS AND METHODS: Sixty-six patients were examined with two single-shot echo-planar diffusion-weighted MR sequences. In the first sequence, liver diffusion isotropy was evaluated by using diffusion gradients in three directions with two *b* values. In the second sequence, a unidirectional diffusion gradient was used with four *b* values. ADCs were measured in 43 patients with 52 focal hepatic lesions more than 1 cm in diameter and in 23 patients with 14 normal and nine cirrhotic livers and were compared by using nonparametric tests.

RESULTS: Diffusion in the liver parenchyma was isotropic. ADCs of focal hepatic lesions were significantly different between sequences ($P < .01$). The mean ($\pm$ SD) ADCs in the first sequence were 0.94×10^{-3} mm^2/sec $\pm$ 0.60 for metastases, 1.33×10^{-3} mm^2/sec $\pm$ 0.13 for HCCs, 1.75×10^{-3} mm^2/sec $\pm$ 0.46 for benign hepatocellular lesions, 2.95×10^{-3} mm^2/sec $\pm$ 0.67 for hemangiomas, and 3.63×10^{-3} mm^2/sec $\pm$ 0.56 for cysts. There was a significant difference between benign (2.45×10^{-3} mm^2/sec $\pm$ 0.96, isotropic value) and malignant (1.08×10^{-3} mm^2/sec $\pm$ 0.50) lesions ($P < .01$ for both sequences).

CONCLUSION: Diffusion-weighted MR imaging can help differentiate benign from malignant hepatic lesions. The use of two *b* values in one direction could be sufficient for the design of MR sequences in the liver.

Diffusion is the thermally induced motion of water molecules in biologic tissues, called Brownian motion (1–3). The microscopic motion includes molecular diffusion of water and microcirculation of blood in the capillary network (microperfusion). With the addition of diffusion gradient pulses, magnetic resonance (MR) imaging—by means of apparent diffusion coefficient (ADC) measurement (1–3)—is currently the best imaging method for in vivo quantification of the combined effects of capillary perfusion and diffusion. The primary application of diffusion-weighted MR imaging has been in brain imaging, mainly for the evaluation of acute ischemic stroke, intracranial tumors, and demyelinating disease (4–8). With the advent of the echo-planar MR imaging technique (9–12), diffusion-weighted MR imaging of the abdomen has become possible with fast imaging times, which minimize the effect of gross physiologic motion from respiration and cardiac movement.

Investigators in a few preliminary studies measured the ADCs of abdominal organs and focal hepatic lesions by using a single-shot echo-planar MR imaging sequence (13–16). Results of these studies showed principally that diffusion-weighted MR imaging, by means of ADC measurement, can be used to characterize focal hepatic lesions. Benign lesions, such as hepatic cysts and hemangiomas, showed higher ADCs than those of malignant lesions (hepatocellular carcinomas [HCCs] and metastases).

Investigators in most previous studies measured the ADC in only one direction and implicitly assumed that, unlike in the brain (4,8) and kidney (17), the diffusion characteristics of the liver are isotropic. In addition, the ADCs of benign hepatocellular lesions, including cases of focal nodular hyperplasia and adenoma, have not yet been reported, to our knowledge.

The purpose of this study was to *(a)* evaluate liver diffusion isotropy, *(b)* compare two single-shot echo-planar diffusion-weighted MR imaging sequences for the characterization of focal hepatic lesions by using two or four *b* values, and *(c)* determine a threshold ADC value to differentiate benign lesions (eg, cysts, hemangiomas, cases of focal nodular hyperplasia, and adenomas) from malignant lesions (eg, HCCs and metastases).

MATERIALS AND METHODS

Patients

The protocol in our study was approved by our institutional review board, and informed consent was obtained from all patients. During a period of 6 months, 66 consecutive patients (33 men and 33 women; mean age, 52 years; age range, 24–79 years) suspected of having hepatic lesions were prospectively examined with diffusion-weighted MR imaging. Among them, 43 patients had 52 focal hepatic lesions (mean diameter, 5 cm; range, 1.0–15.5 cm) evaluated on diffusion-weighted MR images. Nine patients had two lesions, and 34 patients had one lesion. When a patient had different types of lesions, all types were included in the study. In addition, 23 patients had no focal hepatic lesions or had infracentimetric lesions not evaluated at diffusion-weighted MR imaging. Among them, nine patients had cirrhosis related to alcohol intoxication ($n = 5$) or chronic viral hepatitis B ($n = 2$) or C ($n = 2$). The remaining 14 patients had either normal examination results or lesions smaller than 1 cm, without concomitant cirrhosis. The hepatic lesions were separated into five groups.

Metastases.—Fifteen metastatic lesions (mean diameter, 3.4 cm; range, 1.0–8.7 cm) were evaluated in nine patients. The primary tumors were colorectal carcinoma ($n = 6$), carcinoid tumor ($n = 8$) of the gastrointestinal tract or pancreas, and renal carcinoma ($n = 1$). The diagnosis of metastasis was proven by means of surgery, needle biopsy, and follow-up imaging examinations, including ultrasonography (US), computed tomography (CT), and MR imaging, which showed progression of the lesions in two, three, and four patients, respectively. All the metastases were solid, without any cystic component.

HCCs.—Nine HCCs (mean diameter, 4.3 cm; range, 1.5–8.0 cm) were evaluated in nine patients. The diagnosis of HCC was assigned on the basis of MR imaging, CT, or US findings and confirmed by means of histologic findings or the elevation of serum α-fetoprotein levels in four and five patients, respectively. All patients with HCC had concomitant cirrhosis related to chronic viral hepatitis B or C or to hemochromatosis in five, three, and one patient, respectively. The diagnosis of cirrhosis was assigned on the basis of clinical findings in five patients and on the basis of histologic findings in four patients.

Benign hepatocellular lesions.—Fifteen benign hepatocellular lesions (mean diameter, 6.8 cm; range, 2.0–15.5 cm), including 12 cases of focal nodular hyperplasia and three hepatic adenomas, were evaluated in 15 patients. The diagnosis of focal nodular hyperplasia (mean diameter, 6.0 cm; range, 2.0–11.4 cm) was established in the presence of typical MR imaging findings (18) in 12 patients without history of cancer and with normal hepatic function test results. On T2-weighted images, the cases of focal nodular hyperplasia were isointense ($n = 8$) or slightly hyperintense ($n = 4$) when compared with the surrounding normal hepatic tissue. The diagnosis of hepatocellular adenoma (mean diameter, 9.4 cm; range, 4.1–15.5 cm) was assigned at MR imaging (19) in three patients with heterogeneous lesions with some areas of hyperintensity on T2-weighted images; all diagnoses were confirmed by means of surgical resection.

Hemangiomas.—Seven hemangiomas (mean diameter, 3.8 cm; range, 2.1–6.4 cm) were evaluated in seven patients. The diagnosis of hemangioma was established by means of hyperintensity on T2-weighted images and the typical enhancement pattern seen at CT or MR imaging (slightly irregular or globular peripheral enhancement after injection of a bolus of contrast medium, with gradual filling of the center of the lesion on delayed images) (20,21).

Cysts.—Six cysts (mean diameter, 5.5 cm; range, 2.4–8.0 cm) were evaluated in three patients. One patient had adult polycystic renal disease with multiple hepatic cysts. The diagnosis of hepatic cysts was established by means of typical MR imaging findings (hypointense on T1-weighted images and hyperintense on T2-weighted images, with no enhancement after contrast material injection) and US appearances.

MR Imaging

Patients were examined with a 1.5-T superconducting MR system (Gyroscan; Philips Medical Systems, Best, the Netherlands) with a 23 mT/m maximum gradient capability and a surface phased-array coil. All patients underwent diffusion-weighted MR imaging in addition to imaging with a routine hepatic MR protocol to identify and select hepatic lesions suitable for ADC measurement. The protocol included a T1-weighted dual fast gradient-recalled-echo sequence (in-phase and out-of-phase sequences) (repetition time msec/echo time msec, 126/4.6 [in-phase], 2.3 [out-of-phase]; flip angle, 80°; matrix, 179 × 256; section thickness, 8 mm; intersection gap, 2.5 mm; one signal acquired; field of view, 320 mm), a T2-weighted fast spin-echo sequence with spectral fat saturation (1,800/85; fast spin-echo factor, 16; matrix, 512 × 512; section thickness, 8 mm; intersection gap, 2.5 mm; two signals acquired; field of view, 320 mm), and a T1-weighted gradient-echo out-of-phase sequence after dynamic injection of 0.1 mmol per kilogram of body weight of gadoterate meglumine (Dotarem; Guerbet, Aulnay-sous-Bois, France) through a power injector at a rate of 2 mL/sec.

Diffusion-weighted MR Imaging

Before contrast material injection, two breath-hold diffusion-weighted MR sequences were performed with the single-shot echo-planar imaging technique. These sequences combined diffusion gradient pulses before and after the 180° pulse. Spectral fat saturation was used systematically to exclude chemical shift artifacts.

First sequence.—With this sequence, liver isotropy was evaluated by using dif-

TABLE 1
ADCs in the Frequency-encoding (x), Phase-encoding (y), and Section select (z) Directions Obtained with the First Diffusion-weighted MR Sequence (b = 0 and 500 sec/mm^2) in 66 Patients

Tissue or Lesion Type	ADC			*P* Value
	x	y	z	
Normal liver (n = 14)	1.71 ± 0.31	1.83 ± 0.38	1.72 ± 0.29	.61
Cirrhotic liver (n = 9)	1.25 ± 0.50	1.34 ± 0.56	1.27 ± 0.54	.83
Metastatic lesions (n = 15)	0.94 ± 0.66	0.95 ± 0.61	0.93 ± 0.59	.99
HCCs (n = 9)	1.32 ± 0.12	1.34 ± 0.14	1.32 ± 0.27	.79
Benign hepatocellular lesions (n = 15)*	1.68 ± 0.54	1.67 ± 0.31	1.72 ± 0.33	.85
Hemangiomas (n = 7)	2.82 ± 0.57	2.85 ± 0.67	2.93 ± 0.90	.87
Cysts (n = 6)	3.44 ± 0.50	3.43 ± 0.39	3.47 ± 0.56	.95

Note.—Except for *P* values, data are mean ($\times 10^{-3}$ mm^2/sec) ± SD. All *P* values were not significant. n = number of lesions or measurements.
* Includes 12 cases of focal nodular hyperplasia and three adenomas.

TABLE 2
ADCs Obtained with Two Diffusion-weighted MR Sequences in 66 Patients

Tissue or Lesion Type	First Sequence*	Second Sequence†	*P* Value‡
Normal liver (n = 14)	1.83 ± 0.36	1.51 ± 0.49	.06
Cirrhotic liver (n = 9)	1.37 ± 0.52	1.09 ± 0.46	.10
Metastatic lesions (n = 15)	0.94 ± 0.60	0.85 ± 0.51	.60
HCCs (n = 9)	1.33 ± 0.13	1.39 ± 0.24	.48
Benign hepatocellular lesions (n = 15)§	1.75 ± 0.46	1.64 ± 0.33	.53
Hemangiomas (n = 7)	2.95 ± 0.67	2.84 ± 0.71	.38
Cysts (n = 6)	3.63 ± 0.56	2.89 ± 0.83	.28

Note.—Except for *P* values, data are mean ($\times 10^{-3}$ mm^2/sec) ± SD. n = number of lesions or measurements.
* b = 0 and 500 sec/mm^2; $P < .01$ for comparison between ADCs of hepatic lesions and those of normal and cirrhotic livers.
† b = 0–400 sec/mm^2; $P < .01$ for comparison between ADCs of hepatic lesions and those of normal and cirrhotic livers.
‡ *P* values indicate insignificant differences between the two sequences.

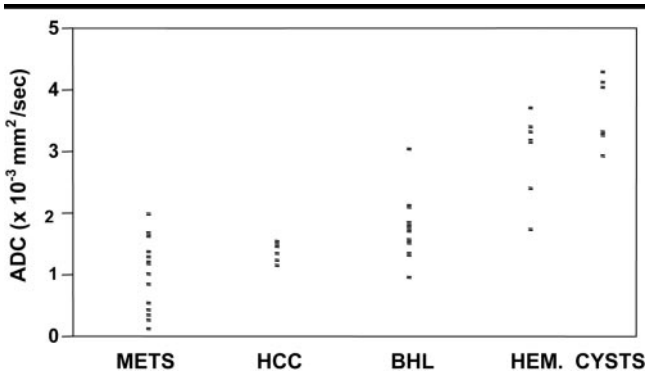

Figure 1. Scatterplot of isotropic ADCs of hepatic metastases *(METS),* HCCs, benign hepatocellular lesions *(BHL),* hemangiomas *(HEM.),* and cysts obtained with the first diffusion-weighted MR sequence.

fusion gradients with two b values (0 and 500 sec/mm^2) along three directions: the frequency-encoding *(x),* phase-encoding *(y),* and section-select *(z)* directions. Five images were obtained: one image for b = 0, one image for each direction for b = 500 sec/mm^2, and one isotropic image. The following parameters were used to acquire 20 sections (two sets of 10 sections each) in a 24-second breath hold: 2,400/104; gradient strength, 20 mT/m; diffusion gradient duration, 26 msec; matrix size, 82 × 128; section thickness, 6 mm; intersection gap, 2 mm; one signal acquired; field of view, 320 mm.

Second sequence.—In this sequence, a unidirectional diffusion gradient was applied along the section-select direction (z axis) with four increasing b values: 0, 134, 267, and 400 sec/mm^2. Four images were obtained (one for each b value). The following parameters were used to acquire 15 sections in a 12-second breath hold: 3,106/104; gradient strength, 20.4 mT/m; diffusion gradient duration, 23.5 msec; matrix size, 128 × 256; section thickness, 8 mm; intersection gap, 3 mm; one signal acquired; field of view, 350 mm.

Phantom studies.—To validate our system, a preliminary phantom study was performed. Plastic tubes filled with water and acetone were imaged with increasing b values: 200, 300, 400, 500, 600, and 1,000 sec/mm^2. The ADCs of water and acetone were calculated at ambient room temperature (21°C).

Image Analysis

All MR images were analyzed retrospectively in consensus by two experienced radiologists (V.V., B.T.) who were aware of the results of CT and US. The focal hepatic lesions were identified on the T1- and T2-weighted images, and their signal intensities, sizes, and patterns of enhancement after contrast material injection were noted. Because of the limited resolution of the diffusion-weighted sequences, only lesions larger than 1 cm in diameter were evaluated. The ADCs were measured in 52 lesions (>1 cm) in 43 patients. Quantitative ADC maps were derived automatically on a voxel-by-voxel basis by using commercially available software (Intera Workstation, release 8.1.3; Philips Medical Systems). The ADC was calculated with a linear regression analysis of the function $S = S_0 \cdot \exp(-b \times \text{ADC})$, where b is the diffusion factor, S is the signal intensity after application of the diffusion gradient, and S_0 is the signal intensity at b = 0 sec/mm^2.

One of the two radiologists (B.T.) established regions of interest in each lesion on the mapping images, and ADC values were obtained by using a workstation (EZ Vision Workstation, release 4; Philips Medical Systems). All regions of interest (round shape, at least 10 mm in

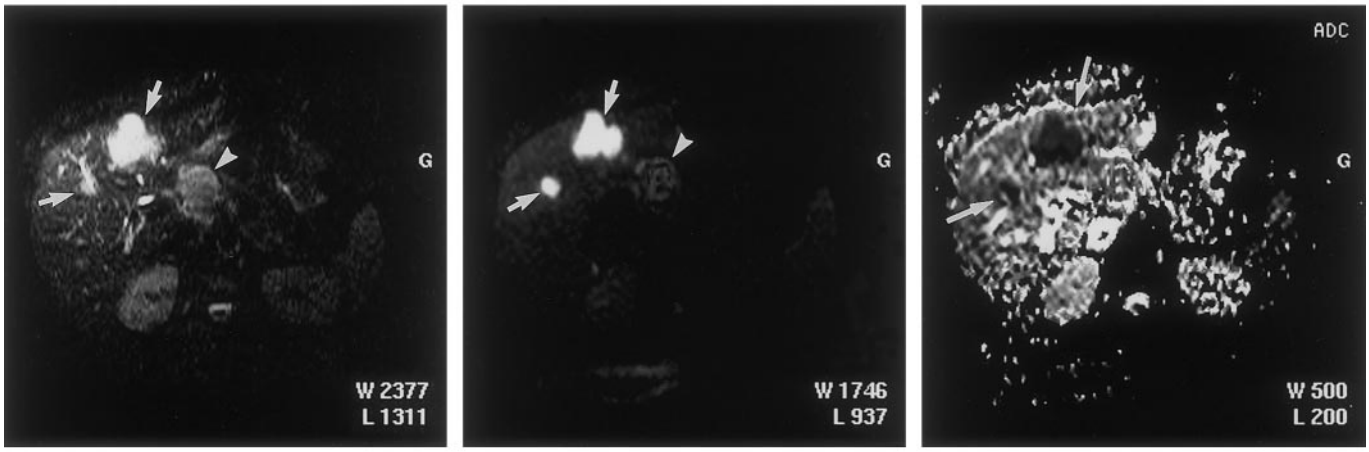

a. b. c.

Figure 2. Images in a 33-year-old man with hepatic metastases from a pancreatic neuroendocrine tumor. Transverse single-shot echo-planar 2,400/104 MR images at **(a)** $b = 0$ sec/mm^2 and **(b)** $b = 500$ sec/mm^2 show hyperintense metastases (arrows) of the right and left hepatic lobes, with no attenuation at $b = 500$ sec/mm^2. The primary tumor (arrowhead) is located in the pancreatic head. **(c)** Mapping image had an ADC of 0.5×10^{-3} mm^2/sec.

diameter) were placed within the confines of the lesions; for heterogeneous lesions, regions of interest included the entire lesion. To ensure that the same areas were measured, the regions of interest were copied and pasted onto the T1-, T2-, and diffusion-weighted MR images and ADC maps. In normal and cirrhotic livers, regions of interest were always placed in the posterior segment of the right hepatic lobe to avoid artifacts from the great vessels. ADCs were each measured twice, and the measurements were averaged.

Statistical Evaluation

To evaluate liver isotropy, ADCs obtained in three directions (frequency encoding, phase encoding, and section select) were compared. To determine the ADCs of focal hepatic lesions and to try to determine whether the ADCs of focal hepatic lesions help differentiate benign from malignant lesions, the ADCs measured in every lesion on MR diffusion-weighted images were compared between the different groups of lesions and between normal and cirrhotic livers. ADCs of normal and cirrhotic livers were also compared for both sequences. In addition, ADCs were compared between both imaging sequences. The Kruskall-Wallis test was used for overall comparison, and the Wilcoxon signed rank test was used for comparison between two groups. The differences were considered significant when P values were less than .05.

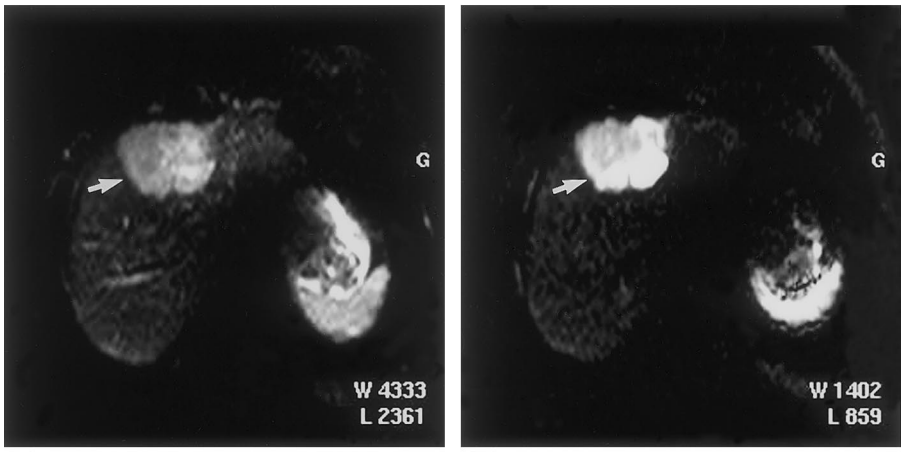

a. b.

Figure 3. Images in a 60-year-old woman with hepatic metastasis from colon carcinoma. Transverse single-shot echo-planar 2,400/104 MR images at **(a)** $b = 0$ sec/mm^2 and **(b)** $b = 500$ sec/mm^2 show hyperintense metastasis (arrow) of the right hepatic lobe, with no attenuation at $b = 500$ sec/mm^2. ADC was 1.34×10^{-3} mm^2/sec.

RESULTS

Phantom Studies

The ADCs of water and acetone were 2.30×10^{-3} mm^2/sec and 4.48×10^{-3} mm^2/sec, respectively, at 21°C. These values were consistent with those reported previously (11,15,22,23).

Patients

ADCs were measured in all focal hepatic lesions included in the study and in 14 normal and nine cirrhotic livers.

Liver isotropy.—The normal and cirrhotic liver parenchyma and all explored focal hepatic lesions were isotropic, with small nonsignificant differences between the ADCs measured in the three directions (Table 1).

ADCs.—The overall comparison of the ADCs of the different groups of lesions and the ADCs of normal and cirrhotic livers (Table 2 and Fig 1) showed a significant difference ($P < .01$) with both imaging sequences. The lowest ADCs were found in metastases (Figs 2, 3) and HCCs (Fig 4), and the highest values were found in hemangiomas (Fig 5) and hepatic cysts (Fig 6). The mean (± SD) isotropic ADCs obtained with the first se-

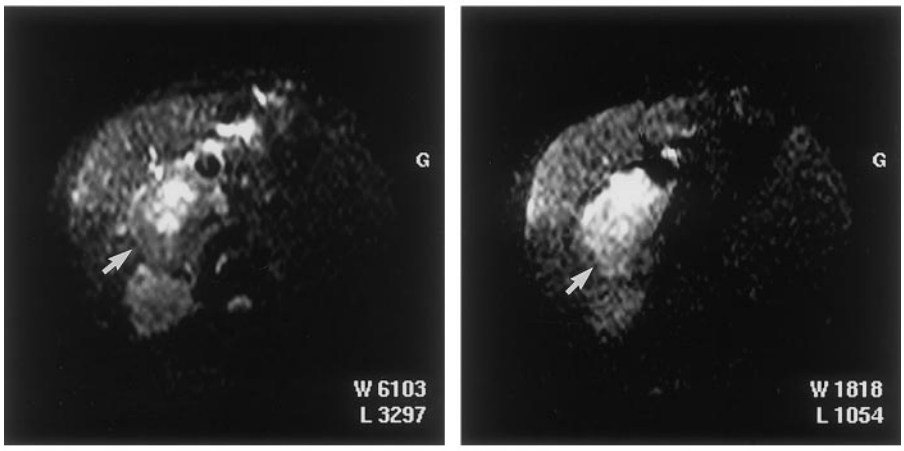

a. b.

Figure 4. Images in a 58-year-old man with HCC of the liver related to chronic hepatitis B. Transverse single-shot echo-planar 2,400/104 MR images at **(a)** $b = 0$ sec/mm^2 and **(b)** $b = 500$ sec/mm^2 show HCC (arrow) of the caudate lobe with central areas of hyperintensity, remaining hyperintense at $b = 500$ sec/mm^2. ADC was 1.31×10^{-3} mm^2/sec.

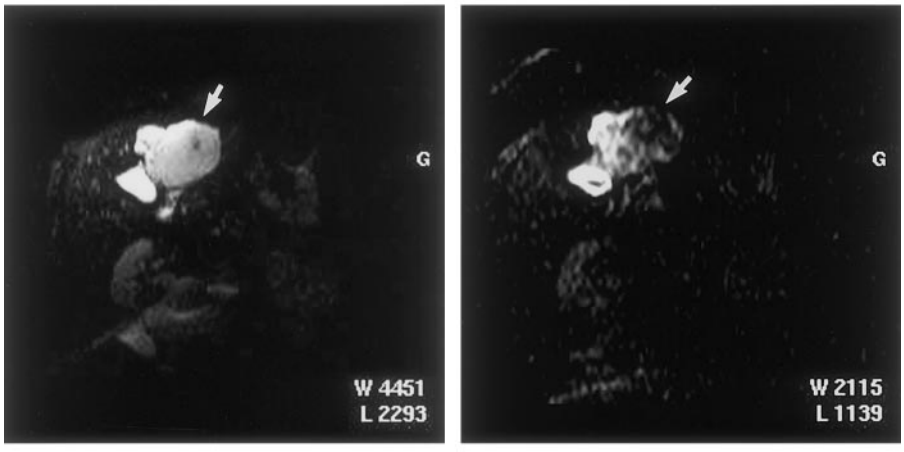

a. b.

Figure 5. Images in a 65-year-old woman with hepatic hemangioma. Transverse single-shot echo-planar 2,400/104 MR images at **(a)** $b = 0$ sec/mm^2 and **(b)** $b = 500$ sec/mm^2 show hyperintense hemangioma (arrow) of the left hepatic lobe at $b = 500$ sec/mm^2. ADC was 3.18×10^{-3} mm^2/sec.

quence ranged from 0.94×10^{-3} mm^2/sec $\pm$ 0.60 for metastases and 1.33×10^{-3} mm^2/sec $\pm$ 0.13 for HCCs to 2.95×10^{-3} mm^2/sec $\pm$ 0.67 for hemangiomas and 3.63×10^{-3} mm^2/sec $\pm$ 0.56 for cysts; benign hepatocellular lesions had intermediate ADCs (1.75×10^{-3} mm^2/sec $\pm$ 0.46). The two-by-two comparison showed a significant difference between all focal hepatic lesions, except between metastases and HCCs with the first sequence ($P = .12$) and cysts and hemangiomas with both sequences ($P = .15$ for the first sequence and $P = .9$ for the second sequence). There was also a significant difference with both sequences between the ADCs of metastases and normal liver ($P < .01$ with the first sequence and $P < .01$ with the second sequence), hemangiomas and normal liver ($P < .01$ for both), hemangiomas and cirrhotic liver ($P < .02$ and $P < .01$), cysts and normal liver ($P < .01$ and $P < .04$), and cysts and cirrhotic liver ($P < .01$ and $P < .05$). There was a significant difference between the ADCs of HCCs and normal liver only with the first sequence ($P < .002$). In addition, there was an insignificant difference between the ADCs of benign hepatocellular lesions and normal liver ($P = .72$ with the first sequence and $P = .24$ with the second sequence).

The ADCs of malignant lesions were significantly lower than those of benign lesions ($P < .01$ with both sequences; Table 3, Fig 7). The ADCs of focal nodular hyperplasia ranged from 1.3 to 3.0×10^{-3} mm^2/sec with the first sequence and from 1.22 to 2.15×10^{-3} mm^2/sec with the second sequence (two cases of focal nodular hyperplasia had ADCs greater than 2×10^{-3} mm^2/sec with both sequences). The ADCs of adenomas ranged from 0.96 to 1.74×10^{-3} mm^2/sec for the first sequence and from 1.06 to 1.66×10^{-3} mm^2/sec for the second sequence. All lesions with an ADC greater than 2×10^{-3} mm^2/sec were benign, and all lesions with an ADC less than 1×10^{-3} mm^2/sec were malignant with both sequences.

Lesions with an ADC between 1 and 2×10^{-3} mm^2/sec were either benign (11 of 15 [73%] and 13 of 15 [86%] benign hepatocellular lesions for the first and second sequences, respectively, and one of seven [14%] hemangiomas with both sequences) or malignant (seven of 15 [46%] metastases and nine of nine [100%] HCCs with both sequences). Use of a threshold ADC value less than 1.5×10^{-3} mm^2/sec for the diagnosis of malignant lesions would result in sensitivity, specificity, positive predictive value, and accuracy of 84% (21 of 25), 89% (24 of 27), 87% (21 of 24), and 86% (45 of 52), respectively, with the first sequence, and 79% (23 of 29), 96% (22 of 23), 96% (23 of 24), and 86% (45 of 52), respectively, with the second sequence.

Comparison of ADCs of normal and cirrhotic livers.—The ADCs of normal liver ranged from 1.40 to 2.55×10^{-3} mm^2/sec (isotropic values) with the first sequence and from 1.12 to 2.71×10^{-3} mm^2/sec with the second sequence, whereas the ADCs of cirrhotic liver ranged from 0.21 to 1.81×10^{-3} mm^2/sec with the first sequence and from 0.17 to 1.48×10^{-3} mm^2/sec with the second sequence. The mean ADCs of cirrhotic liver (Table 2) were significantly lower than those of normal liver ($P < .05$ with both sequences). Despite the statistical difference, however, there was a considerable overlap.

Comparison of the two imaging sequences.—The ADCs of all hepatic lesions (except for HCCs) and normal and cirrhotic livers obtained with the second sequence were slightly lower than those obtained with the first sequence (Tables 2, 3), without reaching statistical significance.

DISCUSSION

Liver Isotropy

To our knowledge, the results of the present study are the first to demonstrate

that the liver, unlike the brain (4,8) and kidney (17), has an isotropic diffusion pattern, probably due to its randomly organized structure. This information indicates that the use of multidirectional diffusion gradients is probably unnecessary for the design of future hepatic diffusion studies.

Characterization of Focal Hepatic Lesions and Differences between the Two Imaging Sequences

Differentiation of benign from malignant hepatic lesions is a frequent diagnostic problem at MR imaging. In our study, we obtained similar results by using two or four *b* values in terms of the characterization of focal hepatic lesions and the differentiation of benign from malignant lesions. The malignant lesions, including metastases and HCCs, had the lowest ADCs, whereas the benign lesions, including hemangiomas and cysts, had the highest ADCs. Benign hepatocellular lesions had intermediate ADCs. To our knowledge, we were the first investigators to explore the ADCs of benign hepatocellular lesions. Previous studies were focused on the differentiation between benign and malignant focal hepatic lesions by measuring the ADCs (11,13–15,24,25), and all of them showed lower ADCs in malignant lesions than those in benign lesions, with variable overlap. Except for one study (24) in which turboFLASH (Siemens, Erlangen, Germany) MR imaging was used, all previous studies (11,13–15) were designed with an echo-planar MR sequence, mostly with single-shot echo-planar MR imaging (13–15). However, the results of these studies showed considerable discrepancies in ADCs for abdominal organs and focal hepatic lesions (Table 4), probably related to the different *b* values, which ranged from very low to very high values (30–1,200 sec/mm^2).

Ichikawa et al (14) probably overestimated the ADCs by using very low *b* values (<55 sec/mm^2). ADCs tend to be higher when using low *b* values, because the signal intensity due to diffusion plays only a minor role in that case (1). On the other hand, the low ADCs reported by Namimoto et al (13) and Yamada et al (25) are probably underestimated because large *b* values (<1,200 and <1,100 sec/mm^2) were used. In our study, we reported overall ADC values close to those reported by Müller et al (11) and Kim et al (15), although ours were slightly higher for normal and cirrhotic livers with the first sequence. As in these two previous studies (11,15), the ADCs were validated in our study by performing phantom measurements. In addition, we proposed a threshold ADC value of 1.5×10^{-3} mm^2/sec, which was close to that proposed by Kim et al (1.6×10^{-3} mm^2/sec) (15) and lower than that proposed by Ichikawa et al (5.5×10^{-3} mm^2/sec) (14).

We found equivalent results for the characterization of focal hepatic lesions and for the differentiation of benign and

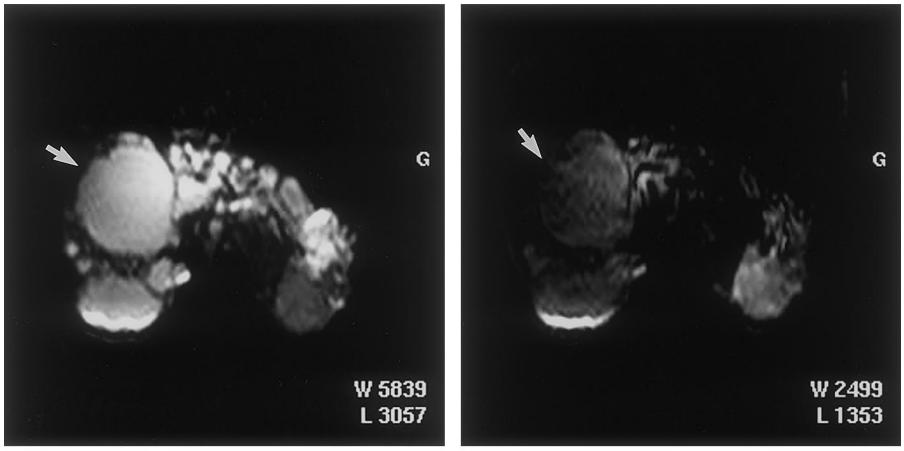

a. **b.**

Figure 6. Images in a 45-year-old woman with adult polycystic renal disease and multiple hepatic cysts. Transverse single-shot echo-planar 2,400/104 MR images at **(a)** $b = 0$ sec/mm^2 and **(b)** $b = 500$ sec/mm^2 show multiple hyperintense cysts of the liver and kidney at $b = 500$ sec/mm^2. ADC of the largest cyst (arrow) was 3.3×10^{-3} mm^2/sec.

TABLE 3
ADCs Obtained with Two Diffusion-weighted MR Sequences in 52 Lesions

Lesions	First Sequence*	Second Sequence†	*P* Value‡
Malignant ($n = 24$)	1.08 ± 0.50	1.06 ± 0.50	.89
Benign ($n = 28$)	2.45 ± 0.96	2.14 ± 0.79	.20

Note.—Except for *P* values, data are mean ($\times 10^{-3}$ mm^2/sec) ± SD. *n* = number of lesions or measurements.
* $b = 0$ and 500 sec/mm^2; $P < .01$ for comparison between malignant and benign lesions.
† $b = 0$–400 sec/mm^2; $P < .01$ for comparison between malignant and benign lesions.
‡ *P* values indicate insignificant differences between the two sequences.

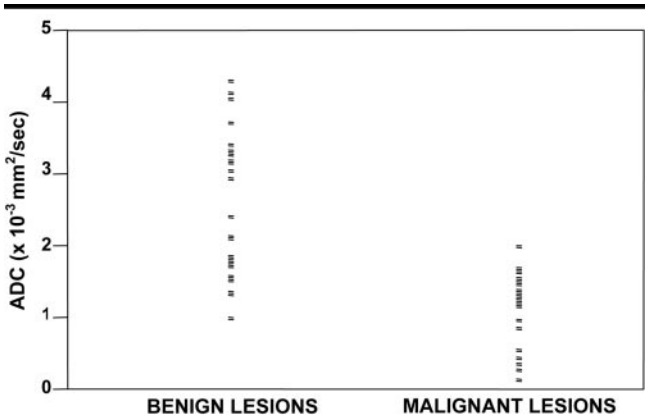

Figure 7. Scatterplot of the isotropic ADCs of malignant and benign focal hepatic lesions obtained with the first diffusion-weighted MR sequence. ADCs of benign and malignant lesions overlap between 1.0 and 2.0×10^{-3} mm^2/sec.

TABLE 4
ADCs Reported in Previous Studies Compared with Those in Our Study

Parameter	Müller et al (11)	Namimoto et al (13)	Ichikawa et al (14)	Kim et al (15)*	Our Study†
No. of Patients	19	51	46	126	66
b value (sec/mm^2)	328–454	30–1,200	<55	<410–<850	<400–500
ADC ($\times 10^{-3}$ mm^2/sec)					
Normal liver	1.39	0.69	2.28	1.02–1.20	1.83–1.51
Cirrhotic liver	0.90–1.20	0.60	1.96	0.88–1.11	1.37–1.09
Metastases	1.20	1.15	2.85	1.06–1.11	0.94–0.85
HCCs	1.70	0.99	3.84	0.97–1.28	1.33–1.39
Hemangiomas	2.00–2.80	1.95	5.39	2.04–2.10	2.95–2.84
Cysts	3.90–5.30	3.05	NA	2.91–3.03	3.63–2.89
Benign hepatocellular lesions	NA	NA	NA	NA	1.75–1.64
Benign lesions	NA	NA	NA	2.49–2.61	2.45–2.14
Malignant lesions	NA	1.04	NA	1.01–1.24	1.08–1.06

Note.—NA = not available.
* The ADCs for $b < 850$ sec/mm^2 and $b < 400$ sec/mm^2 are given.
† The mean ADCs of the first ($b = 0$ and 500 sec/mm^2; isotropic value) and second ($b = 0$–400 sec/mm^2) sequences are given.

malignant lesions by comparing the results with the two diffusion-weighted sequences implemented in our study. However, the ADCs were slightly higher when using *b* values of 0–500 sec/mm^2 than those obtained with *b* values of 0–400 sec/mm^2, without reaching statistical significance. The ADCs obtained with the second sequence were probably more precise than those obtained with the first sequence, because the number of data used for the ADC calculation was increased (four *b* values instead of two). In the study of Kim et al (15), the ADCs obtained with a higher *b* value (<850 sec/mm^2) were lower than those obtained with lower *b* values (<100 and <410 sec/mm^2). In our study, the small difference in the magnitude of the *b* values (100 sec/mm^2) probably did not influence ADC calculation.

In our study, we decided to explore the ADCs of benign hepatocellular lesions, including cases of focal nodular hyperplasia and adenomas, despite their relatively short T2 values, because the lesions included were large (mean size of 6.8 mm) and easily depicted on the diffusion-weighted images. Unsurprisingly, the benign hepatocellular lesions had intermediate ADCs, ranging mostly between 1 and 2×10^{-3} mm^2/sec (except for two cases of focal nodular hyperplasia with ADCs greater than 2×10^{-3} mm^2/sec), which were not different from those of normal liver parenchyma. Despite some overlap, however, benign hepatocellular lesions had significantly different ADCs when compared with those of other hepatic lesions, particularly HCCs.

As in previous studies, we found that hepatic cysts had the highest ADCs because of their fluid content, with nonrestricted motion of water molecules. The ADCs of hemangiomas were also high (all but one had ADCs greater than 2×10^{-3} mm^2/sec) but lower than those of cysts, without reaching statistical significance. This is probably related to the vascular content of hemangiomas, which is more viscous than cystic fluid (13). Moreover, we found that metastatic lesions and HCCs had the lowest ADCs, probably due to their high tumoral content, which restricts the water diffusion. All the metastatic lesions included in our study were solid and did not manifest cystic components that can increase the ADC (13). Hepatic metastases of carcinoid tumors can mimic hemangiomas on T1- and T2-weighted images, and the differentiation between these two lesions usually depends on dynamic gadolinium-enhanced imaging findings (21,26,27). Results of studies (28–30) have shown that T2 measurements can be useful to differentiate hepatic malignancies from hemangiomas and cysts and have questioned the routine use of gadolinium-based contrast material. Diffusion-weighted MR imaging, by means of ADC measurement, is an additional tool that can be used accurately for that purpose.

Finally, as in most previous studies (11,13–15,31), the results of our study showed lower ADCs of cirrhotic liver than those of normal liver, despite a considerable overlap. A possible explanation is the restricted water diffusion in fibrotic liver (11,31).

The present study had several potential limitations, mostly related to the imaging sequences. First, single-shot echo-planar imaging has a low spatial resolution and low signal-to-noise ratio, and therefore, infracentimetric lesions were not evaluated. Findings in recent studies have shown that new fast imaging sequences (32) can improve image quality and decrease echo-planar imaging–related artifacts or that the use of high-field-strength 3.0-T imagers (33) can potentially improve the signal in diffusion-weighted MR imaging. Second, the patient population was relatively small, but an approximately equivalent number of benign ($n = 28$) and malignant lesions ($n = 24$) were evaluated. However, further studies with a larger number of patients are needed in the future. Third, we did not use high *b* values because of the diminished image quality, and overestimation of the ADCs by including the perfusion fraction was possible; however, we did not intend—as in the study of Yamada et al (25)—to measure the true diffusion coefficient. Fourth, despite the significant differences between benign and malignant lesions, there was an overlap of their ADCs between 1 and 2×10^{-3} mm^2/sec, particularly between benign hepatocellular lesions and HCCs.

In summary, we provide evidence that suggests that liver diffusion is isotropic and that diffusion-weighted MR imaging can give additional information for the characterization of hepatic lesions and can potentially be useful for the differentiation between benign and malignant hepatic lesions. A combined use of ADC and T2 measurements may reduce the need for the systematic use of gadolinium-based contrast material at MR imaging. In light of these results, for future clinical applications of diffusion-weighted MR imaging of the liver, we recommend the use of a monodirectional diffusion gradient with a minimum of two *b* values.

Acknowledgment: We thank David Breazale, research assistant, for reviewing the manuscript.

References

1. Le Bihan D, Breton E, Lallemand D, Aubin ML, Vignaud J, Laval-Jeantet M. Separation of diffusion and perfusion in intra-voxel incoherent motion MR imaging. Radiology 1988; 168:497–505.
2. Le Bihan D. Diffusion/perfusion MR imaging of the brain: from structure to function. Radiology 1990; 177:328–329.
3. Le Bihan D, Turner R, Douek P, Patronas N. Diffusion MR imaging: clinical applications. AJR Am J Roentgenol 1992; 159: 591–599.
4. Bammer R, Stollberger R, Augustin M, et al. Diffusion-weighted imaging with navigated interleaved echo-planar imaging and a conventional gradient system. Radiology 1999; 211:799–806.
5. Sorensen AG, Buonanno FS, Gonzalez RG, et al. Hyperacute stroke: evaluation with combined multisection diffusion-weighted and hemodynamically weighted echo-planar MR imaging. Radiology 1996; 199:391–401.
6. Lutsep HL, Albers GW, De Crespigny A, et al. Clinical utility of diffusion-weighted magnetic resonance imaging in the assessment of ischemic stroke. Ann Neurol 1997; 41:574–580.
7. Tsuruda JS, Chew WM, Moseley ME, Norman D. Diffusion-weighted MR imaging of extraaxial tumors. Magn Reson Med 1991; 19:316–320.
8. Schaefer PW, Grant PE, Gonzalez RG. Diffusion-weighted MR imaging of the brain. Radiology 2000; 217:331–345.
9. Butts K, Riederer SJ, Ehman RL, Felmlee JP, Grimm RC. Echo-planar imaging of the liver with a standard MR imaging system. Radiology 1993; 189:259–264.
10. Edelman RR, Wielopolski P, Schmitt F. Echo-planar MR imaging. Radiology 1994; 192:600–612.
11. Müller MF, Prasad P, Siewert B, Nissenbaum MA, Raptopoulos V, Edelman RR. Abdominal diffusion mapping with use of a whole-body echo-planar system. Radiology 1994; 190:475–478.
12. Keogan MT, Edelman RR. Technologic advances in abdominal MR imaging. Radiology 2001; 220:310–320.
13. Namimoto T, Yamashita Y, Sumi S, Tang Y, Takahashi M. Focal liver masses: characterization with diffusion-weighted echo-planar MR imaging. Radiology 1997; 204:739–744.
14. Ichikawa T, Haradome H, Hachiya J, Nitatori T, Araki T. Diffusion-weighted MR imaging with a single-shot echoplanar sequence: detection and characterization of focal hepatic lesions. AJR Am J Roentgenol 1998; 170:397–402.
15. Kim T, Murakami T, Takahashi S, Hori M, Tsuda K, Nakamura H. Diffusion-weighted single-shot echoplanar MR imaging for liver disease. AJR Am J Roentgenol 1999; 173:393–398.
16. Chan JH, Tsui EY, Luk SH, et al. Diffusion-weighted MR imaging of the liver: distinguishing hepatic abscess from cystic or necrotic tumor. Abdom Imaging 2001; 26:161–165.
17. Ries M, Jones RA, Basseau F, Moonen CT, Grenier N. Diffusion tensor MRI of the human kidney. J Magn Reson Imaging 2001; 14:42–49.
18. Vilgrain V, Fléjou JF, Arrivé L, et al. Focal nodular hyperplasia of the liver: MR imaging and pathologic correlation in 37 patients. Radiology 1992; 184:699–703.
19. Arrivé L, Fléjou JF, Vilgrain V, et al. Hepatic adenoma: MR findings in 51 pathologically proved lesions. Radiology 1994; 193:507–512.
20. Quinn SF, Benjamin GG. Hepatic cavernous hemangiomas: simple diagnostic sign with dynamic bolus CT. Radiology 1992; 182:545–548.
21. Semelka RC, Brown ED, Ascher SM, et al. Hepatic hemangiomas: a multi-institutional study on appearance on T2-weighted and serial gadolinium-enhanced gradient-echo MR images. Radiology 1994; 192:401–406.
22. Brockstedt S, Thomsen C, Wirestam R, Holtas S, Stahlberg F. Quantitative diffusion coefficient maps using fast spin-echo MRI. Magn Reson Imaging 1998; 16:877–886.
23. Lorenz CH, Pickens DR III, Puffer DB, Price RR. Magnetic resonance diffusion/perfusion phantom experiments. Magn Reson Med 1991; 19:254–260.
24. Moteki T, Ishikaza H, Horikoshi H, Matsumoto M. Differentiation between hemangiomas and hepatocellular carcinomas with the apparent diffusion coefficient calculated from turboFLASH MR images. J Magn Reson Imaging 1995; 5:187–191.
25. Yamada I, Aung W, Himeno Y, Nakagawa T, Shibuya H. Diffusion coefficients in abdominal organs and hepatic lesions: evaluation with intravoxel incoherent motion echo-planar MR imaging. Radiology 1999; 210:617–623.
26. Berger JF, Laissy JP, Limot O, et al. Differentiation between multiple liver hemangiomas and liver metastases of gastrinomas: value of enhanced MRI. J Comput Assist Tomogr 1996; 20:349–355.
27. Bader TR, Semelka RC, Chiu VC, Armao DM, Woosley JT. MRI of carcinoid tumors: spectrum of appearances in the gastrointestinal tract and liver. J Magn Reson Imaging 2001; 14:261–269.
28. Olcott EW, Li KC, Wright GA, et al. Differentiation of hepatic malignancies from hemangiomas and cysts by T2 relaxation times: early experience with multiply refocused four-echo imaging at 1.5 T. J Magn Reson Imaging 1999; 9:81–86.
29. Fenlon HM, Tello R, deCarvalho VL, Yucel EK. Signal characteristics of focal liver lesions on double echo T2-weighted conventional spin echo MRI: observer performance versus quantitative measurements of T2 relaxation times. J Comput Assist Tomogr 2000; 24:204–211.
30. Tello R, Fenlon HM, Gagliano T, deCarvalho VL, Yucel EK. Prediction rule for characterization of hepatic lesions revealed on MR imaging: estimation of malignancy. AJR Am J Roentgenol 2001; 176:879–884.
31. Amano Y, Kumazaki T, Ishihara M. Single-shot diffusion-weighted echo-planar imaging of normal and cirrhotic livers using a phased-array multicoil. Acta Radiol 1998; 39:440–442.
32. Bammer R, Keeling SL, Augustin M, et al. Improved diffusion-weighted single-shot echo-planar imaging (EPI) in stroke using sensitivity encoding (SENSE). Magn Reson Med 2001; 46:548–554.
33. Hunsche S, Moseley ME, Stoeter P, Hedehus M. Diffusion-tensor MR imaging at 1.5 and 3.0 T: initial observations. Radiology 2001; 221:550–556.